引文格式： *孙斐，卢阳阳，胡静. 离子渗复合处理与单一离子渗氮动力学对比研究[J]. 航空制造技术，2022, 65(15): 59–63.*
SUN Fei, LU Yangyang, HU Jing. Comparative study on plasma complex treatment and plasma nitriding[J]. Aeronautical Manufacturing Technology, 2022, 65(15): 59–63.

离子渗复合处理与单一离子渗氮动力学对比研究*

孙　斐[1]，卢阳阳[2]，胡　静[2]
（1. 常州工业职业技术学院，常州 213164；
2. 常州大学材料科学与工程国家级实验教学示范中心，常州 213164）

[摘要] 为发挥离子渗氮和离子氮碳共渗两种技术各自的优势并克服其不足，研发了离子氮碳共渗与离子渗氮复合处理（以下简称离子渗复合处理），并与单一离子渗氮进行了对比。采用金相显微镜、X 射线衍射仪和显微硬度计对离子渗层厚度、物相、截面硬度进行了测试，并对化合层形成动力学进行了对比分析。结果表明，45 钢经离子渗复合处理后化合层明显厚于单一离子渗氮，化合物层形成效率显著提高，且表层硬度提高。经离子渗复合处理后化合层新增了 Fe_3C 相，且主要物相发生了由 γ′ 相向 ε 相的转变。动力学分析表明，离子渗复合处理化合层形成扩散激活能比单一离子渗氮明显降低，从 179.7 kJ·mol^{-1} 降低到 87.1 kJ·mol^{-1}，同时得出了 45 钢在 783~843 K 温度范围内离子渗氮与离子渗复合处理化合层厚度与温度之间的关系式分别为 $d_{\text{plasma nitriding}}$=exp（15.8–10810/$T$）与 $d_{\text{complex treatment}}$=exp（9.7–5237/$T$）。

关键词： 离子氮碳共渗；离子渗氮；45 钢；化合物层；动力学；扩散
DOI： 10.16080/j.issn1671-833x.2022.15.059

孙　斐
教授，主要研究方向为材料加工及表面工程。

45 钢作为一种优质碳素结构钢，具有低成本和良好的综合力学性能，已广泛应用于工业生产中[1–5]。为进一步扩大其工程应用领域，有必要通过化学热处理改善其耐磨性与耐腐蚀性，以满足不同工作环境的性能要求[6–10]。常用的化学热处理方法有离子渗碳[11–14]、离子渗氮[15–17]、盐浴渗氮[18]及离子氮碳共渗等[19–20]。相比于其他表面改性技术，离子氮碳共渗技术具有无污染、渗速快、渗层易控制等一系列优点[21–23]，适用于碳素钢、合金钢、不锈钢等材料[1,24]。

离子渗氮和离子氮碳共渗技术是化学热处理领域研究和应用的热点，其中离子渗氮可获得具有良好性能的致密渗层，但工艺周期长、生产效率有待进一步提高；离子氮碳共渗虽然效率比单一离子渗氮提高，但渗层容易出现疏松[5,8]。基于离子渗氮和离子氮碳共渗技术各自的特点，本课题组探索了将两者复合，达到发挥两者优势，并克服各自不足的有利效果[25]。

基于此，本研究采用离子氮碳共渗与离子渗氮复合处理对 45 钢进行表面改性，并与单一离子渗氮进行对比研究，重点是对比离子渗复合处理与单一离子渗氮的动力学特性，旨在为该创新方法的工程实际应用提供指导。

* **基金项目：** 国家自然科学基金（21978025）；江苏省第三期优势学科建设项目（PAPD–3）；江苏高校品牌专业建设工程资助项目（TAPP）；江苏省研究生科研与实践创新计划项目（SJCX22_1327、KYCX22_2979）。

1 试验及方法

试验材料为调质态 45 钢，其化学成分（质量分数）C 为 0.43%~0.45%，Si 为 0.17%~0.37%，Mn 为 0.5%~0.8%，S 为 0.031%，P 为 0.031%，余量为 Fe。采用线切割加工成尺寸为 10 mm × 10 mm × 10 mm 的试样，试样表面先用 SiC 砂纸进行打磨，再用金刚石研磨膏抛光至镜面，最后置于无水乙醇中进行超声波清洗 10~15 min，烘干，密封保存。

离子渗复合处理主要由以下 3 部分组成：（1）将试样置于离子氮化炉中，抽真空至 10 Pa 以下，通入氢气溅射 30 min，炉内压力保持 300 Pa；（2）溅射结束后，通入氮气，氮气流量为 500 mL/min；（3）当炉温升高至设定温度（783~843 K）后，通入丙烷，氮气与丙烷流量分别为 591 mL/min 和 9 mL/min，进行离子氮碳共渗，保温 3 h 后，关闭丙烷，进行离子渗氮，保温 1 h，即离子渗复合处理总时间为 4 h，之后试样随炉冷却至室温。作为对比，采用相同温度范围和相同时间进行单一离子渗氮。

采用 DMI–3000M 型光学金相显微镜观察试样截面显微组织；采用 D/max–2500 型 X 射线衍射仪测试物相组成，使用 Cu–Kα 射线，波长为 λ=1.54 Å，扫描速度设为 0.2°/min，步宽设定为 0.02°，2θ 范围选定为 20°~100°；采用 HXD–1000TMC 型显微硬度计测量截面显微硬度，加载载荷为 0.05 kgf，加载时间为 15 s。

2 结果与讨论

2.1 显微组织与渗层厚度

图 1 为 45 钢经不同方法不同工艺处理后的截面显微组织。可以看出，两种方法都遵循相同的规律：随着温度升高，化合层厚度均呈逐渐增大的趋势。同时发现，在相同处理温度下，45 钢经离子渗复合处理获得的化合层厚度明显大于离子渗氮，这主要是由于碳的加入使气氛中氮势提高，促进了化合层的形成与增长。同时，温度越高，两者化合层厚度差距越大，产生这一现象的原因可能是温度升高使气氛中活性原子的分解和扩散速率加快，促进氮化物形成。可见，45 钢经离子渗复合处理后化合物层形成效率显著提升。

2.2 XRD 物相分析

图 2 为 45 钢离子渗氮与离子渗复合处理（783 K/4 h）后 XRD 衍射谱。可见，离子渗氮后化合层主要物相为 ε 相和 γ′ 相，而离子渗复合处理后化合层中新增了 Fe_3C 相。根据 Fe–N–C 相图可知，Fe_3C 相的出现是由于气氛中碳浓度超过了碳原子在 α–Fe 中的最大溶解度，导致 Fe_3C 的形成 [26]。同时还可以看出，经离子

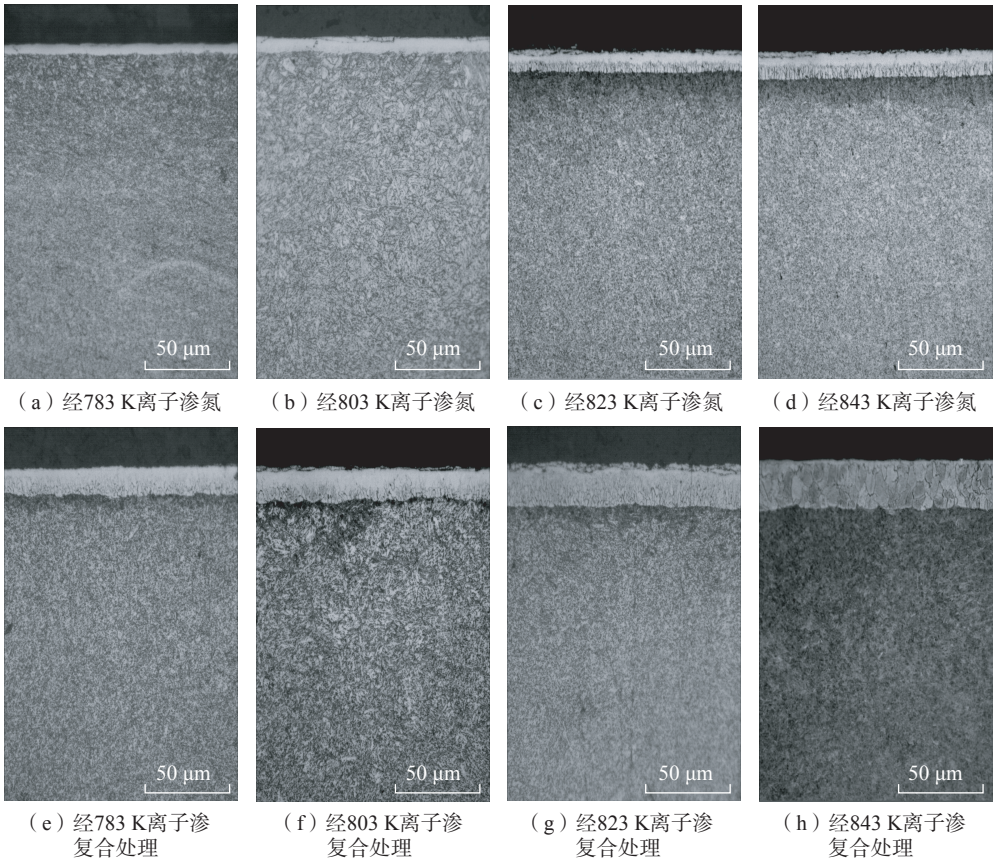

（a）经783 K离子渗氮　（b）经803 K离子渗氮　（c）经823 K离子渗氮　（d）经843 K离子渗氮

（e）经783 K离子渗复合处理　（f）经803 K离子渗复合处理　（g）经823 K离子渗复合处理　（h）经843 K离子渗复合处理

图 1　45 钢经不同方法不同工艺处理后截面显微组织

Fig.1　Cross-sectional microstructure of 45 steel after different processes

渗复合处理后 ε 相衍射峰强度增加，而 γ′ 相衍射峰强度逐渐变小，由此可知，化合层中的主要物相发生了由 γ′ 相向 ε 相的转变，这主要是由于碳的加入，使晶格发生膨胀，碳原子扩散进入基体中并置换其中的氮原子，促进了 ε 相的形成 [22]。

2.3 截面硬度分析

图 3 为 45 钢离子渗氮与离子渗复合处理（783 K/4 h）后的截面硬度曲线，可以看出，随着距离的增加，硬度逐渐下降，最终趋于平缓。45 钢经离子渗复合处理后截面硬度最大值为 $788HV_{0.05}$，比普通离子渗氮后获得的截面硬度提高约 40%。由图 2 可知，这主要是由于离子渗复合处理后渗层中出现较多 ε 相所致。可以看出，普通离子渗氮后有效硬化层约为 35 μm，而复合处理后有效硬化层显著提高，达到约 70 μm。

2.4 动力学分析

图 4 为 45 钢经离子渗氮与离子渗复合处理后化合层生长动力学曲线。可以看出在相同温度下，45 钢离子渗复合处理后化合层厚度明显大于单一离子渗氮，且随温度升高，两者的化合物层厚度差距逐渐增大，843 K/4 h 离子渗复合处理后化合层厚度为 33.2 μm，比单一离子渗氮化合层厚度增加约 80%。

由于离子氮碳共渗与离子渗氮复合处理时化合层的生长是依靠氮、碳原子扩散来完成的，而对于扩散控制过程，扩散系数、激活能及温度满足 Arrhenius 公式，即

$$\ln d=A-(Q/2RT) \quad (1)$$

式中，d 为化合物层厚度，μm；A 为扩散常数；Q 为扩散激活能，kJ/mol；R 为气体常数，8.314 J/（mol·K）；T 为温度，K。

由式（1）可知，扩散激活能 Q 取决于 $\ln d$ 与 $1/T$ 直线关系的斜率，因此，根据图 4 中化合层厚度可以得出 45 钢经离子渗氮与复合处理后的 $\ln d$ 与 $1/T$ 线性拟合关系，如图 5 所示。由图 5 拟合得出的直线方程可得 45 钢不同工艺处理后形成化合层的扩散激活能 Q 和扩散常数 A，如表 1 所示。

将表 1 所列 Q 和 A 数值代入 Arrhenius 公式，就可得出本试验条件下（保温时间为 4 h）45 钢离子渗氮与离子渗复合处理时化合层厚度与保温温度之间的关系表达式，即

$$d_{\text{plasma nitriding}}=\exp(15.8-10810/T) \quad (783\ \text{K} \leqslant T \leqslant 843\ \text{K}) \quad (2)$$

$$d_{\text{complex treatment}}=\exp(9.7-5237/T) \quad (783\ \text{K} \leqslant T \leqslant 843\ \text{K}) \quad (3)$$

根据式（2）和（3）可以预测某一温度下离子渗氮或离子渗复合处理不同时间获得的化合层厚度；同时，为获得设计要求的化合层厚度，可以计算出需要采用的离子渗氮或离子渗复合处理工艺条件，从而为离子渗氮与离子渗复合处理技术的实际应用提供理论和试验依据。

3 结论

（1）45 钢经离子氮碳共渗与离子渗氮复合处理后形成的化合层厚

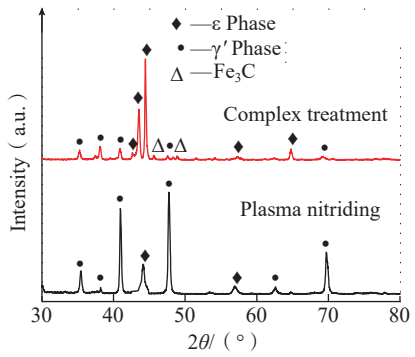

图 2 45 钢离子渗氮与离子渗复合处理（783 K/4 h）后 XRD 衍射谱

Fig.2 XRD patterns of 45 steel after plasma nitriding and complex treatment (783 K/4 h)

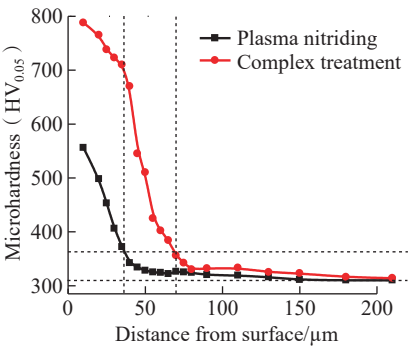

图 3 45 钢离子渗氮与离子渗复合处理（783 K/4 h）后的截面显微硬度

Fig.3 Cross-sectional microhardness of 45 steel after plasma nitriding and complex treatment（783 K/4 h）

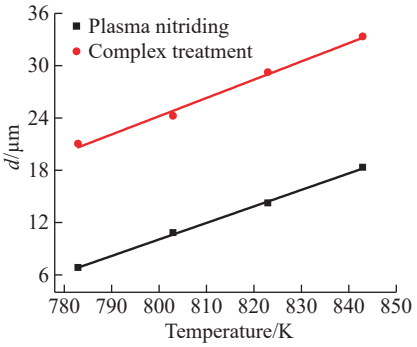

图 4 45 钢经离子渗氮与离子渗复合处理后化合物层生长动力学曲线

Fig.4 Compound layer thickness vs. temperature after plasma nitriding and complex treatment for 45 steel

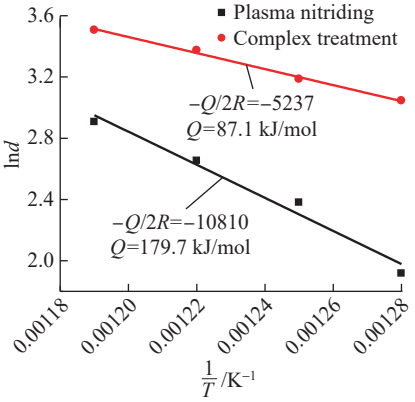

图 5 45 钢经离子渗氮与离子渗复合处理后 $\ln d$ 与 $1/T$ 线性拟合关系

Fig.5 Plot of $\ln d$ vs. $1/T$ after plasma nitriding and complex treatment for 45 steel

表 1 45 钢化合物层形成扩散激活能 Q 和扩散常数 A

Table 1 Activation energy Q and diffusion constant A of compound layer for 45 steel

工艺方法	扩散激活能 Q/(kJ·mol^{-1})	扩散常数 A
Plasma nitriding	179.7	15.8
Complex treatment	87.1	9.7

度比单一离子渗氮显著提高。

（2）离子渗氮后渗层中主要物相为ε相和γ′相，而离子氮碳共渗与离子渗氮复合处理后渗层中新增了Fe_3C，且发生了由γ′相向ε相的转变。

（3）离子氮碳共渗与离子渗氮复合处理可显著提高45钢渗层硬度，表层最大硬度达到788$HV_{0.05}$，比单一离子渗氮截面硬度提高约40%，且有效硬化层显著提高。

（4）45钢经离子氮碳共渗与离子渗氮复合处理后化合层形成扩散激活能显著降低，从单一离子渗氮的179.7 kJ/mol降低到87.1 kJ/mol。

（5）获得了45钢在783~843 K温度范围内离子氮碳共渗与离子渗氮复合处理后化合层厚度与温度之间的关系式分别为$d_{\text{plasma nitriding}}=\exp(15.8-10810/T)$，$d_{\text{complex treatment}}=\exp(9.7-5237/T)$。

参 考 文 献

[1] GAO K, QIN X P, WANG Z, et al. Effect of spot continual induction hardening on the microstructure of steels: Comparison between AISI 1045 and 5140 steels[J]. Materials Science and Engineering: A, 2016, 651: 535–547.

[2] LIU R L, QIAO Y J, YAN M F, et al. Effects of rare earth elements on the characteristics of low temperature plasma nitrocarburized martensitic stainless steel[J]. Journal of Materials Science & Technology, 2012, 28(11): 1046–1052.

[3] LIU H, LI J C, CHAI Y T, et al. A novel plasma oxynitriding by using plain air for AISI 1045 steel[J]. Vacuum, 2015, 121: 18–21.

[4] CAI W, MENG F N, GAO X Y, et al. Effect of QPQ nitriding time on wear and corrosion behavior of 45 carbon steel[J]. Applied Surface Science, 2012, 261: 411–414.

[5] LEE I. The effect of molybdenum on the characteristics of surface layers of low temperature plasma nitrocarburized austenitic stainless steel[J]. Current Applied Physics, 2009, 9(3): S257–S261.

[6] ORJUELAG A, RINCóN R, OLAYA J J. Corrosion resistance of niobium carbide coatings produced on AISI 1045 steel via thermo-reactive diffusion deposition[J]. Surface and Coatings Technology, 2014, 259: 667–675.

[7] WANG B, JIN X Y, XUE W B, et al. High temperature tribological behaviors of plasma electrolytic borocarburized Q235 low-carbon steel[J]. Surface and Coatings Technology, 2013, 232: 142–149.

[8] DE ARA J F, ALMANDOZ E, PALACIO J F, et al. Influence of temperature in arc-activated plasma nitriding of maraging steel in solution annealed and aged conditions[J]. Surface and Coatings Technology, 2014, 258: 754–762.

[9] 缪小吉，武计强，梅文臣，等. 42CrMo钢离子氮氧共渗与离子渗氮对比研究[J]. 航空制造技术，2019, 62(21): 64–68.

MIAO Xiaoji, WU Jiqiang, MEI Wenchen, et al. Comparative study on plasma oxynitriding and plasma nitriding for 42CrMo steel[J]. Aeronautical Manufacturing Technology, 2019, 62(21): 64–68.

[10] MISHRA S C, MOHANTY B C, NAYAK B B. Arc plasma nitriding of low carbon steel[J]. Surface and Coatings Technology, 2001, 145(1–3): 24–30.

[11] CHEN F S, WANG K L. Super-carburization of low alloy steel and low carbon steel by fluidized-bed furnaces[J]. Surface and Coatings Technology, 2000, 132(1): 36–44.

[12] ZHANG J, HU Y, TAN X J, et al. Microstructure and high temperature tribological behavior of laser cladding Ni60A alloys coatings on 45 steel substrate[J]. Transactions of Nonferrous Metals Society of China, 2015, 25(5): 1525–1532.

[13] SCHEUER C J, CARDOSO R P, PEREIRA R, et al. Low temperature plasma carburizing of martensitic stainless steel[J]. Materials Science and Engineering: A, 2012, 539: 369–372.

[14] SCHEUER C J, CARDOSO R P, ZANETTI F I, et al. Low-temperature plasma carburizing of AISI 420 martensitic stainless steel: Influence of gas mixture and gas flow rate[J]. Surface and Coatings Technology, 2012, 206(24): 5085–5090.

[15] XI Y T, LIU D X, HAN D. Improvement of corrosion and wear resistances of AISI 420 martensitic stainless steel using plasma nitriding at low temperature[J]. Surface and Coatings Technology, 2008, 202(12): 2577–2583.

[16] SUN Y, BELL T. Low temperature plasma nitriding characteristics of precipitation hardening stainless steel[J]. Surface Engineering, 2003, 19(5): 331–336.

[17] ALLENSTEIN A N, LEPIENSKI C M, BUSCHINELLI A J A, et al. Plasma nitriding using high H2 content gas mixtures for a cavitation erosion resistant steel[J]. Applied Surface Science, 2013, 277: 15–24.

[18] YEĞEN İ, USTA M. The effect of salt bath cementation on mechanical behavior of hot-rolled and cold-drawn SAE 8620 and 16MnCr5 steels[J]. Vacuum, 2010, 85(3): 390–396.

[19] YAN M F, LIU R L, WU D L. Improving the mechanical properties of 17–4PH stainless steel by low temperature plasma surface treatment[J]. Materials & Design, 2010, 31(4): 2270–2273.

[20] YAN M F, LIU R L. Martensitic stainless steel modified by plasma nitrocarburizing at conventional temperature with and without rare earths addition[J]. Surface and Coatings Technology, 2010, 205(2): 345–349.

[21] QIANG Y H, GE S R, XUE Q J. Microstructure and tribological properties of complex nitrocarburized steel[J]. Journal of Materials Processing Technology, 2000, 101(1–3): 180–185.

[22] YE X M, WU J Q, ZHU Y L, et al. A study of the effect of propane addition on plasma nitrocarburizing for AISI 1045 steel[J]. Vacuum, 2014, 110: 74–77.

[23] 戴达煌，周克松，袁镇海. 现代材料表面技术科学[M]. 北京：冶金工业出版社，2004.

DAI Dahuang, ZHOU Kesong, YUAN Zhenhai. Surface technology science of modern material[M]. Beijing: Metallurgical Industry Press, 2004.

[24] ALPHONSA J, RAJA V S, MUKHERJEE S. Development of highly hard and corrosion resistant A286 stainless steel through plasma nitrocarburizing process[J]. Surface and Coatings Technology, 2015, 280: 268–276.

[25] 缪斌，李景才，孙泉，等. 离子氮碳共渗与离子渗氮复合处理对45钢组织与性能的影响[J]. 中国表面工程，2016, 29(4): 30–34.

MIAO Bin, LI Jingcai, SUN Quan, et al. Effects of complex treatment of plasma nitrocarburizing and plasma nitriding on microstructure and properties of 45 steel[J]. China Surface Engineering, 2016, 29(4): 30–34.

[26] EBRAHIMI M, MAHBOUBI F, NAIMI-JAMAL M R. Wear behavior of DLC film on plasma nitrocarburized AISI 4140 steel by pulsed DC PACVD: Effect of nitrocarburizing temperature[J]. Diamond and Related Materials, 2015, 52: 32–37.

通讯作者：胡静，教授，博导，主要研究方向为金属表面改性及金属热处理。

Comparative Study on Plasma Complex Treatment and Plasma Nitriding

SUN Fei[1], LU Yangyang[2], HU Jing[2]
(1. Changzhou Institute of Industry Technology, Changzhou 213164, China;
2. National Experimental Demonstration Center for Materials Science and Engineering, Changzhou University, Changzhou 213164, China)

[ABSTRACT] In order to take advantage of the individual advantages of plasma nitriding and plasma nitrocarburizing, and overcome their shortcomings, plasma complex treatment combining both plasma nitrocarburizing and plasma nitriding (hereinafter referred to as complex treatment) was developed and compared with a single plasma nitriding. The nitrided layer thickness, phase microstructure, cross-sectional microhardness were investigated by means of optical microscope, X–ray diffraction and microhardness tester. The results show that the compound layer thickness after complex treatment is much thicker than that after plasma nitriding, thus the nitriding efficiency is improved remarkably. Fe_3C phase was occurred in compound layer after complex treatment, and the dominated phase of the compound layer was transformed from γ′ to ε phase. Higher microhardness was obtained after a complex treatment. In addition, activation energy (Q) of forming compound layer decreases from 179.7 kJ/mol in plasma nitriding to 87.1 kJ/mol for the complex treatment. And the kinetics of plasma nitriding and complex treatment in the temperature range of 783 K to 843 K was obtained as the following formula $d_{\text{plasma nitriding}}=\exp(15.8–10810/T)$, $d_{\text{complex treatment}}=\exp(9.7–5237/T)$.

Keywords: Plasma nitrocarburizing; Plasma nitriding; 45 steel; Compound layer; Kinetics; Diffusion

（责编　古京）

（上接第 58 页）

Study on Surface of Nickel Base Superalloy Strengthened by Coupled Ultrasonic and Electric Pulse With Water-in-Oil Working Fluid

JIN Hui, JI Renjie, WANG Baokun, LIU Yonghong
(China University of Petroleum (East China), Qingdao 266580, China)

[ABSTRACT] In this paper, a new type of water-in-oil (W/O) emulsion suitable for coupling electrical pulse and ultrasonic treatment was developed, and the influence of water content on the viscosity and conductivity of the W/O emulsion was explored. It is found that when the water content is 40% and below, the W/O emulsion can maintain low electrical conductivity, have excellent dielectric properties, and better flow properties. Inconel 718 alloy was treated with water, W/O emulsion with mass fraction of 20% and 40%, and the surface morphology, wear resistance and corrosion resistance after treatment were investigated. The results showed that the surface of the sample treated with W/O emulsion with mass fraction of 40% is the smoothest, and has the best wear resistance and corrosion resistance. Compared with the substrate, the friction coefficient is reduced by 0.267, the wear loss is reduced by 43.2%, the corrosion current density is reduced by 86.9%, and the impedance is increased by 45.4%. The W/O emulsion can effectively fill the gap between the carbon brush and the sample, avoid the occurrence of discharge phenomenon. At the same time, the W/O emulsion can provide excellent lubrication effect, which can weaken the friction between ultrasonic vibration head and sample surface, and finally obtains better surface quality.

Keywords: Inconel 718 alloy; Ultrasonic processing; Electric pulse; Water-in-oil working fluid; Wear resistance; Corrosion resistance

（责编　古京）